ChemComm

COMMUNICATION

View Article Online
View Journal | View Issue

Cite this: *Chem. Commun.*, 2015, **51**, 11868

Received 7th May 2015,
Accepted 18th June 2015

DOI: 10.1039/c5cc03822g

www.rsc.org/chemcomm

Biocompatible organic charge transfer complex nanoparticles based on a semi-crystalline cellulose template†

Atsushi Nagai,‡*[ab] Jason B. Miller,‡[b] Jia Du,[c] Petra Kos,[b] Mihaela C. Stefan[c] and Daniel J. Siegwart*[b]

Using a bio-inspired cellulose template, new charge transfer (CT) nanoparticles (NPs) with unique and intriguing emission properties are reported. Pyrene-modified 2,3-di-*O*-methyl cellulose formed CT complexes with small molecule acceptors, *e.g.* 7,7,8,8-tetracyanoquinodimethane (TCNQ), and exhibited aggregation-induced emission (AIE) in aqueous medium upon nanoparticle formation. The TCNQ-CT NPs showed multicolor fluorescence emissions at 370–400 nm, 602 nm and 777 nm, when excited at 330 nm, 485 nm and 620 nm respectively. The cellulose-TCNQ NPs are biocompatible and demonstrate an advance in the use of the CT mechanism for biomedical imaging applications both *in vitro* and *in vivo*.

Herein, we provide evidence that a semi-crystalline template composed of cellulose chemically bearing charge transfer (CT) complexes consisting of pyrene donors and TCNQ (7,7,8,8-tetracyanoquinodimethane), TCNB (1,2,4,5-tetracyanobenzene), and TCNE (tetracyanoethylene) acceptors emit multi-colored fluorescence in solution and in biological settings. Non-covalent organic complexes with electron donor (D) and electron acceptor (A) moieties have emerged as promising candidates for advanced materials with diverse applications (including mechanochromic materials) due to their intermolecular CT capability. This endows the materials with charge ordering, spin density waves (SDW), and superconductivity.[1] Fused arene molecules such as pyrene and coronene have been commonly employed as donors and can donate electrons depending on their ionization potential, *I*.[2] TCNQ is a classic acceptor for organic CT complexes because it can be easily reduced to form the open shell electron radical anion $TCNQ^{-}$ when it comes into contact with electron donors.[3] Pyrene–TCNQ complexes have been shown to crystallize in a monoclinic system with a spacing group of $P2_1/n$ with half of the molecules of pyrene and TCNQ as asymmetric parts of the unit cell, in which the pyrene moiety is tilted with respect to TCNQ along stacks and at an angle between mean planes of 6°.[4] Recently, we demonstrated the first example of mechanochromic conjugated CT materials using pyrene as a donor and TCNQ or TCNB as two acceptors into π-conjugated oligomer backbones.[3] The conjugated materials showed interesting color change from bright orange to metallic deep green upon mechanical grinding in the solid state at room temperature, which was reversible by sonication in toluene. However, this property was lost in solution. To overcome this limitation, we envisioned ordering the CT complexes into a templated design, on a polymer backbone to promote enhanced tumor retention for imaging applications. It is known that the modular structure of CT complexes coupled with environmental dependence on CT properties allows the control over crystal structure and optical properties by alternating CT interactions between electron donors and acceptors. Because small molecule CT complex particles have shown utility in biomedical imaging,[2] we were inspired to design CT complexes based on supramolecular self-assembly of natural polymers, which would enable enhanced tumor retention for *in vivo* imaging applications. Therefore, we selected the semi-crystalline cellulose fiber template as a bio-inspired candidate to control the orientation and interaction of donor and acceptor molecules in the CT complex state.

Bio-inspired materials with unique and intriguing functionalities, such as the self-cleaning ability of plants in nature, have attracted much attention for the rational design of next-generation materials.[5,6] Polymers can be used as a template to construct ordered bio-inspired structures such as helical objects because of their facile processability, low cost, and well defined architecture.[7–10] Cellulose is one of the most abundant biopolymers and has been converted into functional fibers,[11] hydrogels,[12] films,[13] and microspheres.[14] Given its self-assembly properties, we were inspired to utilize cellulose as a semi-crystalline support for not only higher ordering of the active CT complexes, but also a biocompatible platform to develop a new

[a] *Institute for Molecular Science, National Institutes of Natural Sciences, Department of Materials Molecular Science, 5-1 Higashiyama, Myodaiji, Okazaki 444-8787, Japan. E-mail: nagai@ims.ac.jp*
[b] *The University of Texas Southwestern Medical Center, Simmons Comprehensive Cancer Center, Department of Biochemistry, Dallas, Texas 75390, USA. E-mail: daniel.siegwart@utsouthwestern.edu*
[c] *The University of Texas at Dallas, Department of Chemistry and Biochemistry, Richardson, Texas 75080, USA*

† Electronic supplementary information (ESI) available: Equipment, materials, methods and additional Fig. S1–S13 and Tables S1 and S2. See DOI: 10.1039/c5cc03822g

‡ A.N. and J.B.M. contributed equally.

biomedical imaging modality. This communication reports the preparation of new cellulose templated CT complexes. The blue and red emission of CT complexes appended to a cellulose support was further enhanced by using nanoprecipitation, forming nanoparticles with an aggregation-induced emission (AIE) effect. Furthermore, due to the biocompatible nature of the CT emission-active material, the cellulose-CT NPs were nontoxic to cells *in vitro* and could be used for biological imaging in tumors *in vivo*.

To enable control over the environment of the CT complex, the donor molecule, pyrene, was conjugated to a cellulose backbone. 2,3-di-*O*-methyl cellulose (DOMC) was prepared according to the literature[15] and analyzed by gel permeation chromatography (GPC) which showed a monomodal peak (M_n = 27 190, M_w/M_n = 3.12). Pyrene-conjugated DOMC (Py-DOMC) was prepared from the esterification reaction of DOMC with 1-pyrenebutanoyl chloride (Scheme 1), which allowed isolation of Py-DOMC in 60% yield. The conversion of the 6-hydroxyl group of DOMC to the pyrenebutyl ester was confirmed using IR spectroscopy which showed a C=O stretching frequency at 1737 cm^{-1}, and ^1H NMR, which showed broad peaks in the aromatic region (7.49–8.37 ppm) attributable to the pyrene moiety (Fig. S1 and S2, ESI†). Additionally, GPC analysis (Fig. S3, ESI†) showed a monomodal peak for Py-DOMC (M_n = 39 440, M_w/M_n = 3.30), and the increase in molecular weight is indicative of the esterification reaction.

Next, we conducted the CT-coating reaction of Py-DOMC with three acceptors, 7,7,8,8-tetracyanoquinodimethane (TCNQ), tetracyanoethylene (TCNE), or 1,2,4,5-tetracyanobenzene (TCNB), in the mixed solvent of toluene/DMAc (9 : 1 v : v, conc. 0.02 M or 0.2 M) under solvothermal conditions (Scheme 1). After 48 h, the precipitates were collected by centrifugation, washed with excess ethanol, and dried under vacuum at 50 °C to afford the expected CT complex-coated Py-DOMC in 49–51% (0.02 M) and 64–70% (0.2 M) yields. The different yields of the CT-coated Py-DOMC were a result of solvent dependency. As shown in Scheme 1, performing the CT-coating reaction at higher concentration (0.2 M) allows intermolecular CT complex formation, resulting in the physical cross-linking between Py-DOMC strands, as evidenced by noticeably reduced solubility in DMSO. On the contrary, the CT reaction in dilute mixed solvent (0.02 M) showed completely homogeneous deep color solutions such as deep green (TCNQ), pale yellow (TCNE), and orange (TCNB), implying that CT-coating reaction of Py-DOMC using only TCNQ progressed efficiently (Fig. S4, ESI†) to form linear polymers.

IR spectroscopy analysis of the solid CT complexes confirmed the CT complex formation, as indicated by the shift of the CN stretching frequency in comparison to the analogous frequency in the neutral acceptor monomers.[15] Linear TCNQ-CT exhibited a CN stretching frequency of 2218 cm^{-1}, assigned to the formation of CT complexes, as compared to TCNQ monomer (2230 cm^{-1}). Meanwhile, linear TCNE-CT showed a very weak broad peak around 2220 cm^{-1}, which indicates poor complex formation, likely due to lower electron affinity (Fig. S5, ESI†). The IR spectra of cross-linked TCNQ-CT showed bimodal CN stretching at 2217 cm^{-1} and 2183 cm^{-1} while, interestingly at the higher concentration, TCNE-CT showed a broad band at 2216 cm^{-1}, indicating that reaction at high concentration enables both CT-coating and cross-linking (intermolecular and intramolecular reactions between pyrene and acceptors). While TCNB monomer showed a defined CN stretching frequency at 2245 cm^{-1}, neither linear nor cross-linked TCNB-CT had any peaks in this region, which can be attributed to higher steric hindrance as compared to TCNQ and TCNE.

Thermal degradation behavior of all CT complexes was examined by thermogravimetric analysis (TGA) (Fig. S6 and Table S1, ESI†). Evidence of the cross-linking was apparent when comparing the TGA curve of the CT complexes when formed at high or low concentration. For TCNQ-CT cellulose, the final weight percent (T = 500 °C) for the high concentration complex was 44.03% while the low concentration complex was 32.49%, which confirms the cross-linked conformation of the CT complex. The same trend was observed for TCNE-CT cellulose ($wt\%_{final}$ linear 28.15%, cross-linked 37.49%). Meanwhile, for TCNB, the final weight percent of the linear form was 31.45% while the cross-linked form was 28.05%. This suggests that no cross-linking occurred, likely due to the steric hindrance of this acceptor.

The UV-vis absorptions of Py-DOMC, TCNQ-, TCNE-, and TCNB-CT-linear cellulose relative to monomeric TCNQ, TCNE, and TCNB, respectively were examined in DMSO solution (Fig. 1). The acceptors exhibited absorption maxima at 400 (TCNQ), 300 (TCNE), and 317 (TCNB) nm, respectively, and only TCNQ showed two broad bands between at 651 and 889 nm. Vibration absorption maxima at 345 nm of TCNQ-, TCNB-, and TCNQ-CT-celluloses red-shifted from that of Py-DOMC at 341 nm (Fig. S8, ESI†). TCNQ-CT-cellulose showed

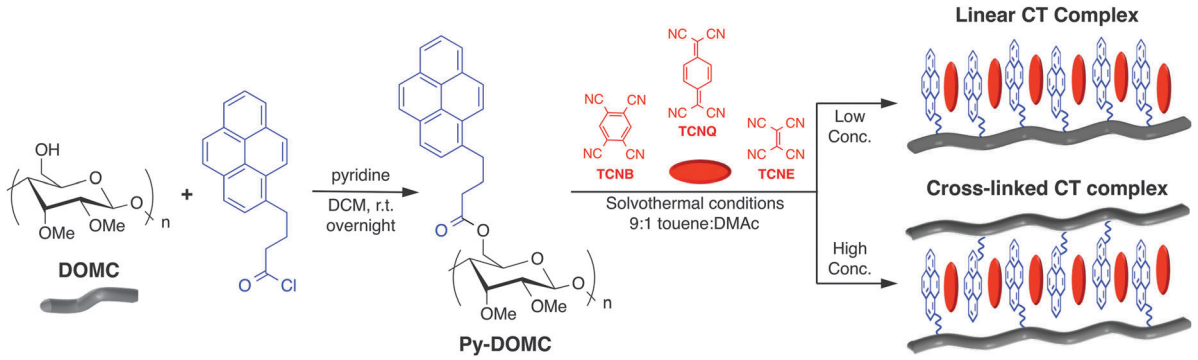

Scheme 1 Synthesis of methyl cellulose bearing pyrene donor molecules (Py-DOMC) and the formation of CT complexes with TCNQ, TCNB, and TCNE acceptors, yielding linear (low concentration, 0.02 M) or cross-linked (high concentration, 0.2 M) materials.

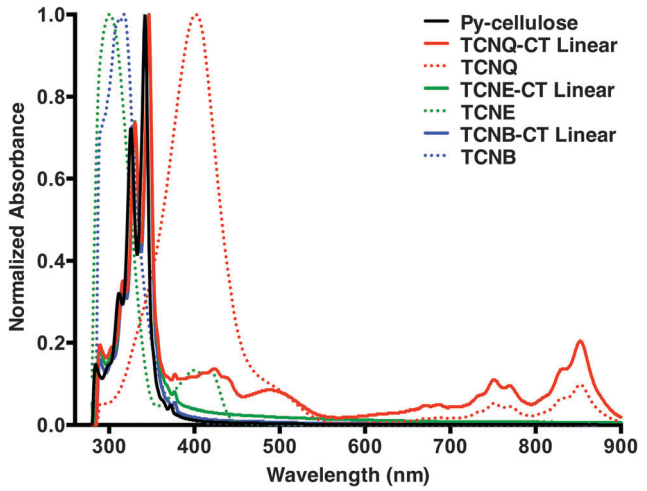

Fig. 1 Normalized absorption spectra of Py-, TCNQ-, TCNE-, and TCNB-CT-celluloses relative to monomeric TCNQ, TCNE, and TCNB in DMSO solution (c = 0.1 g L^{-1}).

broad bands in the red to near IR region, which overlap with monomeric TCNQ. Consequently, the CT cellulose has no typical CT bands at high wavelength in DMSO. These data show that slight red shifts of pyrene moieties on the cellulose indicate weak CT π-stacking interaction that was influenced by the highly ordered cellulose-based fiber. Interestingly, upon sonication of the DMSO solution of TCNQ-CT, the peak at 345 nm reverts back to the peak at 345 nm reverts back to 341 nm and the high wavelength peaks disappear, suggesting wavelength peaks disappear, suggesting disruption of the weak π–π stacking interactions (Fig. S9, ESI†).

To generate improved CT-cellulose absorbance and emission properties, we employed the AIE approach to increase aggregation interactions between donors and acceptors by forming nanoparticles of the CT complexes. TCNQ-CT-cellulose nanoparticles were formed by nanoprecipitation to improve the ordering form in the cellulose bearing pyrene and TCNQ pair.[16] For this purpose, 100 μL TCNQ-CT cellulose (c = 1 g L^{-1} in DMSO) was added drop wise to deionized water (900 μL) under stirring. The size of the resulting nanoparticles was 36 ± 4 nm as measured by dynamic light scattering (DLS) (Fig. S10 and Table S2, ESI†). Fig. 2 shows UV-vis and fluorescence spectra of TCNQ-CT-cellulose nanoparticles (TCNQ-CT NP) in aqueous solution, as compared to Py-DOMC NPs. Because NPs formed from TCNE-CT and TCNB-CT did not show any new absorbance peaks, these were not further analyzed (Fig. S11, ESI†).

Fig. 2a shows the UV spectra of TCNQ-CT-cellulose NPs, Py-DOMC NPs, and a TCNQ suspension in aqueous solution (0.02 g L^{-1}). TCNQ-CT-cellulose NPs exhibit two distinct broad absorbance bands at 485 and 620 nm, which can be differentiated from the bands of TCNQ monomer. These new broad peaks are due to formation of the CT complex.[17] The semi-crystalline cellulose template helps in order to maintain regular CT stacking structure between pyrene and TCNQ. Next, photoluminescence (PL) experiments of TCNQ-CT-cellulose NPs compared to Py-DOMC NPs were carried out in aqueous solution containing a small amount of DMSO (0.01 or 0.02 g L^{-1}). Decrease of the excimer emission peak of the pyrene moiety at 450 nm results in the CT reformation by nanoprecipitation suggesting

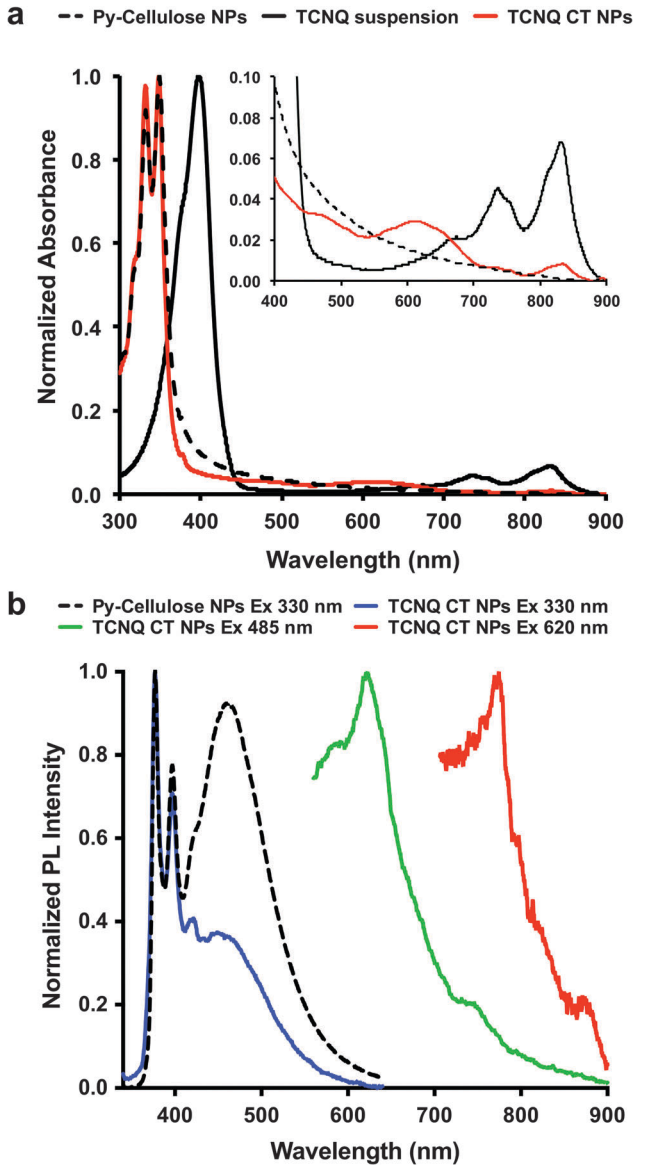

Fig. 2 (a) UV-vis absorption of TCNQ-CT-cellulose NPs, Py-DOMC NPs, and a TCNQ suspension. (b) Photoluminescence of TCNQ-CT-cellulose NPs in aqueous solution (0.02 g L^{-1}).

that the aggregation state inhibits high order array of the CT complexes in the NP. However, the active CT nanoparticle formed between TCNQ and pyrene moieties in the cellulose emits blue light at 376–540 nm. Interestingly, TCNQ-CT-cellulose nanoparticle showed efficient red emission at 602 nm upon the excitation of 485 nm (CT first broad band maximum). In addition, excitation at 620 nm results in a small emission peak at 777 nm.

Because we are interested in the potential for these cellulose-based CT NPs to be used in biomedical imaging, we next measured the cytotoxicity of the NPs to cells *in vitro*. TCNQ-CT-cellulose NPs were incubated with HeLa cells at different concentrations and cell viability was quantified using the CellTitre-Glo assay. TCNQ-CT-cellulose NPs were non-toxic to cells at the concentrations tested (Fig. S12, ESI†).

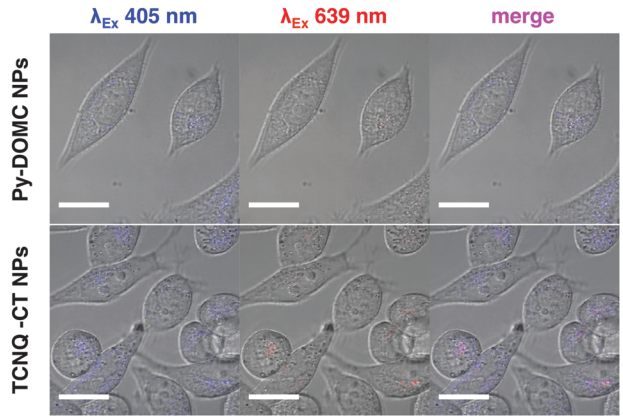

Fig. 3 Cellular uptake of TCNQ-CT-cellulose NPs into HeLa cells *in vitro*. TCNQ-CT-cellulose NPs show red emission after excitation at 639 nm, while Py-DOMC NPs do not. Scale bar = 20 μm.

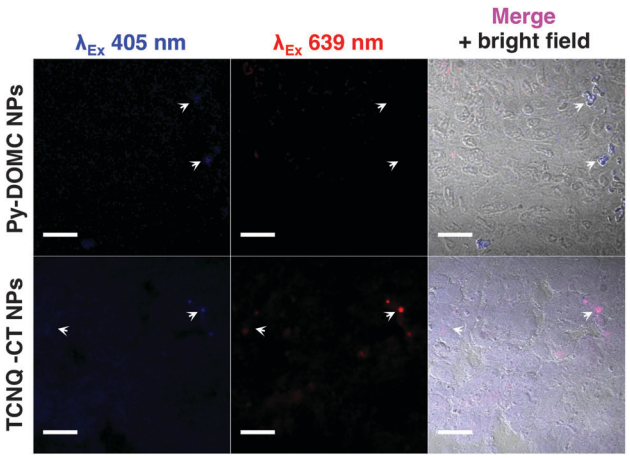

Fig. 4 Imaging of TCNQ-CT-cellulose NPs *in vivo* in mice bearing RPMI-7951 melanoma xenograft tumors. Arrows indicate regions of concentrated NPs. Scale bar = 20 μm.

Next, we explored the potential for the CT mechanism to be preserved in biological settings *in vitro* and *in vivo*. TCNQ-CT-cellulose NPs were stabilized by coating with Tween 20 to reduce NP aggregation. They were added to growing HeLa cells and then imaged after 3 hours of incubation in a proof-of-principle experiment. Fig. 3 shows effective cell uptake of TCNQ-CT-cellulose NPs into HeLa cells. The complexes were imaged using the excitation of the pyrene moiety (λ_{Ex} 405 nm) and near the absorbance of the CT complexes (λ_{Ex} 639 nm). Excitation of the pyrene moiety resulted in strong intracellular signal for both TCNQ-CT and Py-DOMC NPs. Red emission was only observable for the TCNQ-CT NPs, suggesting successful CT. Importantly, the CT mechanism was preserved in serum-containing media.

Finally, we injected TCNQ-CT-cellulose NPs into mice bearing RPMI-7951 melanoma xenograft tumors to test whether CT could be used as an imaging principle *in vivo*. After 4 hours, tumors were harvested, embedded, frozen, and sectioned. Confocal microscopy was used to image the tumor sections (Fig. 4). The results show that TCNQ-CT-cellulose NPs likely aggregated after injection, but that the CT mechanism was preserved. Similar to the *in vitro* results, red emission was observable for the TCNQ-CT NPs. This is suggestive of successful CT *in vivo* after delivery of TCNQ-CT NPs. It is worth noting that the emission was particularly strong in areas of aggregation. Therefore, these TCNQ-CT-cellulose NPs that utilize AIE for effective CT represent a significant advancement for the use of CT complexes for biomedical imaging.

In conclusion, we report the synthesis of new CT complexes based on ordered cellulose biomaterials. Appending CT complexes onto a cellulose backbone enabled control of the orientation and environment of the donor and acceptor molecules of the CT complexes, thus arranging the pyrene–TCNQ interactions to allow detectable absorption and emission properties. This led to unique charge transfer emission properties in the red to near infrared regions. This paper demonstrates that by using an AIE approach through nanoparticle formation, the CT mechanism can occur in biologically relevant conditions *in vitro* and *in vivo*, suggesting future utility of this mechanism for a variety of biomedical imaging applications.

A.N. gratefully acknowledges support from Professor Ohmine Iwao, the Director-General of the Institute for Molecular Science (IMS) in Japan. D.J.S. acknowledges grant support from the Cancer Prevention and Research Institute of Texas (CPRIT) (R1212) and the Welch Foundation (I-1855). J.B.M. acknowledges fellowship support from CPRIT (RP140110). M.C.S. acknowledges grant support from the Welch Foundation (AT-1740), the NSF (Career DMR-0956116), and the NSF-MRI (CHE-1126177).

Notes and references

1 J.-L. Brédas, D. Beljonne, V. Coropceanu and J. Cornil, *Chem. Rev.*, 2004, **104**, 4971–5004.
2 M. D. Gujrati, N. S. S. Kumar, A. S. Brown, B. Captain and J. N. Wilson, *Langmuir*, 2011, **27**, 6554–6558.
3 A. Nagai and Y. Okabe, *Chem. Commun.*, 2014, **50**, 10052–10054.
4 M. A. Dobrowolski, G. Garbarino, M. Mezouar, A. Ciesielski and M. K. Cyranski, *CrystEngComm*, 2014, **16**, 415–429.
5 P. Roach, N. J. Shirtcliffe and M. I. Newton, *Soft Matter*, 2008, **4**, 224–240.
6 T. Sun, L. Feng, X. Gao and L. Jiang, *Acc. Chem. Res.*, 2005, **38**, 644–652.
7 K. Bleek and A. Taubert, *Acta Biomater.*, 2013, **9**, 6283–6321.
8 L. J. Bonderer, A. R. Studart and L. J. Gauckler, *Science*, 2008, **319**, 1069–1073.
9 M. Ma, L. Guo, D. G. Anderson and R. Langer, *Science*, 2013, **339**, 186–189.
10 A. Thomas, F. Goettmann and M. Antonietti, *Chem. Mater.*, 2008, **20**, 738–755.
11 J. Cai, L. Zhang, J. Zhou, H. Qi, H. Chen, T. Kondo, X. Chen and B. Chu, *Adv. Mater.*, 2007, **19**, 821–825.
12 M. He, Y. Zhao, J. Duan, Z. Wang, Y. Chen and L. Zhang, *ACS Appl. Mater. Interfaces*, 2014, **6**, 1872–1878.
13 H. Qi, C. Chang and L. Zhang, *Green Chem.*, 2009, **11**, 177–184.
14 X. Luo, S. Liu, J. Zhou and L. Zhang, *J. Mater. Chem.*, 2009, **19**, 3538–3545.
15 X. Chi, C. Besnard, V. K. Thorsmølle, V. Y. Butko, A. J. Taylor, T. Siegrist and A. P. Ramirez, *Chem. Mater.*, 2004, **16**, 5751–5755.
16 S. Hornig, T. Heinze, C. R. Becer and U. S. Schubert, *J. Mater. Chem.*, 2009, **19**, 3838–3840.
17 R. J. Dillon and C. J. Bardeen, *J. Phys. Chem. A*, 2012, **116**, 5145–5150.